

Metadata of the article that will be visualized in OnlineFirst

ArticleTitle	Mapping the elemental distribution in archaeological findings through advanced Neutron Resonance Transmission Imaging	
Article Sub-Title		
Article CopyRight	The Author(s), under exclusive licence to Società Italiana di Fisica and Springer-Verlag GmbH Germany, part of Springer Nature (This will be the copyright line in the final PDF)	
Journal Name	The European Physical Journal Plus	
Corresponding Author	FamilyName	Marcucci
	Particle	
	Given Name	Giulia
	Suffix	
	Division	Dipartimento di Fisica "G. Occhialini"
	Organization	Università degli Studi di Milano Bicocca and INFN, Sezione di Milano Bicocca
	Address	Piazza della Scienza 3, 20126, Milan, Italy
	Division	
	Organization	ISIS Neutron and Muon Source
	Address	Chilton-Didcot, OX11 0QX, UK
	Phone	
	Fax	
	Email	giulia.marcucci@unimib.it
	URL	
	ORCID	http://orcid.org/0000-0001-9538-7591
Author	FamilyName	Scherillo
	Particle	
	Given Name	Antonella
	Suffix	
	Division	
	Organization	ISIS Neutron and Muon Source
	Address	Chilton-Didcot, OX11 0QX, UK
	Phone	
	Fax	
	Email	
	URL	
	ORCID	http://orcid.org/0000-0002-5294-9416
Author	FamilyName	Riccardi
	Particle	
	Given Name	Maria Pia
	Suffix	
	Division	Dipartimento di Scienze della Terra e dell' Ambiente and Arvedi Laboratorio– sede di Pavia
	Organization	Università degli Studi di Pavia
	Address	via Ferrata 9, 27100, Pavia, Italy
	Phone	
	Fax	
	Email	
	URL	
	ORCID	
Author	FamilyName	Cucini
	Particle	
	Given Name	Costanza
	Suffix	
	Division	IRAMAT, UMR 7065, CNRS
	Organization	Université de Technologie Belfort Montbéliard
	Address	90010, Belfort Cedex, France
	Phone	
	Fax	
	Email	
	URL	
	ORCID	http://orcid.org/0000-0001-5476-9681

Author	FamilyName Particle Given Name Suffix Division Organization Address Phone Fax Email URL ORCID	Lemasson Quentin Ministère de la Culture/Chimie ParisTech 14 Quai François Mitterrand, 75001, Paris, France
Author	FamilyName Particle Given Name Suffix Division Organization Address Phone Fax Email URL ORCID	Martino Di Daniela Dipartimento di Fisica “G. Occhialini” Università degli Studi di Milano Bicocca and INFN, Sezione di Milano Bicocca Piazza della Scienza 3, 20126, Milan, Italy http://orcid.org/0000-0003-1541-5236
Schedule	Received Revised Accepted	23 Dec 2023 28 Apr 2024
Abstract	<p>This work highlights recent application of energy-selective neutron imaging at the ISIS Neutron and Muon Source, specifically focusing on the development of Neutron Resonance Transmission Imaging (NRTI) at the INES instrument. NRTI is a nuclear technique based on resonant neutron absorption reaction, which combines the sensitivity to elemental and isotopic composition with detailed morphological information, using the epithermal portion of the neutron flux available on the INES instrument at the ISIS facility. Unlike standard neutron radiography and tomography methods, NRTI preserves detailed time and energy information for each detector pixel, enabling enhanced visualisation of elemental distribution inside an object’s volume, with the potential for quantitative elemental analysis. These features combined with the non-destructiveness of NRTI make the method promising for applications in the field of Cultural Heritage, especially when it is employed in a multi-technique approach to provide complementary information about the composition and the crystalline structure of archaeological artefacts. A study related to Heritage Science is presented to demonstrate the effectiveness of NRTI in non-destructive investigations of inhomogeneous artefacts, specifically focusing on the excavation finds related to the first evidence of ancient brass production in Milan, Italy, during Roman times.</p>	
Footnote Information		



Mapping the elemental distribution in archaeological findings through advanced Neutron Resonance Transmission Imaging

Giulia Marcucci^{1,2,a}, Antonella Scherillo², Maria Pia Riccardi³, Costanza Cucini⁴, Quentin Lemasson⁵, Daniela Di Martino¹

¹ Dipartimento di Fisica “G. Occhialini”, Università degli Studi di Milano Bicocca and INFN, Sezione di Milano Bicocca, Piazza della Scienza 3, 20126 Milan, Italy

² ISIS Neutron and Muon Source, Chilton-Didcot OX11 0QX, UK

³ Dipartimento di Scienze della Terra e dell’Ambiente and Arvedi Laboratorio– sede di Pavia, Università degli Studi di Pavia, via Ferrata 9, 27100 Pavia, Italy

⁴ IRAMAT, UMR 7065, CNRS, Université de Technologie Belfort Montbéliard, 90010 Belfort Cedex, France

⁵ Ministère de la Culture/Chimie ParisTech, 14 Quai François Mitterrand, 75001 Paris, France

Received: 23 December 2023 / Accepted: 28 April 2024

© The Author(s), under exclusive licence to Società Italiana di Fisica and Springer-Verlag GmbH Germany, part of Springer Nature 2024

Abstract This work highlights recent application of energy-selective neutron imaging at the ISIS Neutron and Muon Source, specifically focusing on the development of Neutron Resonance Transmission Imaging (NRTI) at the INES instrument. NRTI is a nuclear technique based on resonant neutron absorption reaction, which combines the sensitivity to elemental and isotopic composition with detailed morphological information, using the epithermal portion of the neutron flux available on the INES instrument at the ISIS facility. Unlike standard neutron radiography and tomography methods, NRTI preserves detailed time and energy information for each detector pixel, enabling enhanced visualisation of elemental distribution inside an object’s volume, with the potential for quantitative elemental analysis. These features combined with the non-destructiveness of NRTI make the method promising for applications in the field of Cultural Heritage, especially when it is employed in a multi-technique approach to provide complementary information about the composition and the crystalline structure of archaeological artefacts. A study related to Heritage Science is presented to demonstrate the effectiveness of NRTI in non-destructive investigations of inhomogeneous artefacts, specifically focusing on the excavation finds related to the first evidence of ancient brass production in Milan, Italy, during Roman times.

1 Introduction

In recent years, neutron imaging established its strengths and extraordinary versatility for non-destructive investigation of many kinds of morphological and microstructural properties of materials [1–9], as proved by the increase in its availability at neutron sources worldwide, providing fully complementary information concerning conventional imaging techniques based on other probes such as X-rays [10–16]. The rapid development of neutron imaging methods and detection systems has led to a striking improvement in resolution and efficiency, as well as in techniques based on a broad range of contrast mechanisms, making imaging with neutron beams indispensable in modern research.

As a result of their intrinsic properties, neutrons interact with matter differently with respect to electrons, protons or X-rays: due to their neutral charge, they interact when in short-range proximity ($\sim 10^{-15}$ m) with the nucleus of an atom, resulting in a highly penetrating capability of the order of centimetres, depending on the material. This feature has three important consequences: (i) neutrons can be used to investigate microscopic properties of dense matter non-destructively; (ii) they can be used as a bulk probe of matter, overcoming issues related to surface effects/structures, and (iii) and to investigate objects in complex sample environments.

Moreover, neutrons are an optimum probe for observing light atoms, such as hydrogen, as well as for distinguishing neighbour elements in the periodic table. In addition, they are the only scattering probes able to provide isotopic contrast.

The current state of the art of neutron imaging techniques is highly advanced. This work, in particular, aims to provide details into the recent advancement of the 4D Neutron Resonance Transmission Imaging (NRTI) technique [17–19] developed at the INES beamline of the ISIS spallation neutron source [20–22]. Conventionally, neutron imaging often uses cold or thermal neutron beams. However, another rather promising energy range not yet widely used for imaging purposes is the epithermal range, which is exploited for the NRTI technique. High epithermal neutron fluxes are available at neutron spallation sources, enabling the isotopic and elemental characterisation of materials thanks to the presence of intense peak structures (called resonances) in the neutron-induced

^a e-mail: giulia.marcucci@unimib.it (corresponding author)

46 reaction cross sections. The NRTI technique is based on the resonant absorption of the incident epithermal neutrons, resulting in a
47 transmitted neutron beam containing characteristic dips univocally related to the material's elemental and isotopic composition.

48 What sets NRTI apart from standard neutron radiography/tomography is the possibility to conduct simultaneously three-
49 dimensional (3D) mapping with spectroscopic information (4D) and potentially quantitative imaging. In fact, for phenomena based
50 on resonant neutron capture, the absorption of neutrons is the dominant interaction and the relative cross section can be exactly
51 calculated; therefore, quantitative analysis is possible. Moreover, NRTI enables the enhancement of the contrast of specific elements
52 compared to others (in particular those with similar neutron attenuation coefficients for standard tomography) inside the bulk of an
53 object, thanks to the full energy spectrum acquired in each detector pixel. Furthermore, this technique is one of the first imaging
54 methods that can be used for isotopic imaging.

55 In this work, a study related to Cultural Heritage is presented to describe the unique features of NRTI for investigating with
56 enhanced contrast and isotopic sensitivity the elemental composition and distribution inside archaeological objects, especially those
57 with inhomogeneous structures. These characteristics, combined with the non-destructive nature of the method, make NRTI a
58 promising and powerful imaging tool for applications in the field of Heritage Science, expanding the potential of neutron imag-
59 ing and providing complementary information to other more conventional techniques for non-destructive characterisation of an
60 archaeological object.

61 2 Archaeological framework

62 In 2009, the excavation in Corso of Porta Romana 20, Milan (Italy), conducted by *Soprintendenza Archeologia, Belle Arti e Paesaggio*
63 *di Milano*, unearthed numerous fragments of metals slug and crucibles related to brass production and datable between the end of I
64 and the beginning of II century CE [23]. These excavation finds are the first evidence of at least one brass workshop activity in the
65 ancient Roman city of Mediolanum [23, 24]. In fact, brass production was widespread throughout the Roman Empire [25] and well
66 documented in England, Germany and France [26–28], but it was completely unknown in Italy.

67 These crucibles consist of mass-produced terracotta pots, coated with a thick layer of refractory clay. Inside, traces of copper
68 and zinc heating can be found, as they were brought to high temperatures to liquefy the alloy and to throw it into moulds to produce
69 brass appliques for furniture and ornamental objects.

70 A subset of the unearthed crucible fragments clearly shows metallic deposition on their surfaces while in others brass or, more
71 generally, metallic inclusions can be inside their bulk.

72 Therefore, to disclose evidence of brass casting and confirm the composition of the metallic traces in a non-destructive way, from
73 a set of about twenty crucible fragments, eight of them have been selected based on their size (a few centimetres of thickness), weight
74 (as a rough indication of the presence of metallic inclusions in the volume) and superficial morphological properties to request access
75 for elemental analysis through neutron resonance absorption spectroscopy (described in Sect. 3) at the INES beamline of the ISIS
76 Neutron and Muon Source (UK). Considering the thickness of some centimetres, these samples may be opaque to conventional
77 elemental techniques (such as X-ray fluorescence or Particle-Induced X-ray Emission); therefore, neutron techniques have been
78 chosen as the method of analysis to access the composition deeper in the sample volumes.

79 3 Methods

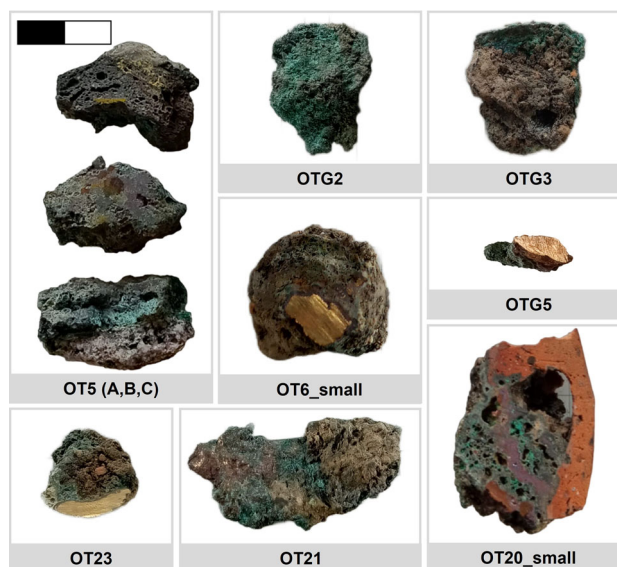
80 NRTI is a spectroscopic method that relies on the interaction of neutrons via resonant absorption with the nuclei present in the
81 sample. The analytical approach is based on the presence of intense peaks, known as resonances, in the neutron-induced reaction
82 cross sections corresponding to an increased probability of absorption at specific neutron energies by several orders of magnitudes.
83 The energy position of resonances differs for each nuclide, allowing for simultaneous elemental and isotopic identification for
84 compositional analysis [29].

85 Two analytical techniques based on this type of interaction, NRCA and NRTI, have been exploited to investigate non-destructively
86 the elemental composition and distribution of the Roman crucible finds, providing bulk information.

87 Both methods are based on Time-Of-Flight (TOF) measurements with epithermal neutrons (0.5 eV–10 keV), exploiting the
88 pulsed nature of the ISIS Neutron and Muon Source.

89 NRCA, as well as NRTI, relies on well-established methodologies. NRCA is an optimised technique both conceptually and
90 experimentally at ISIS to obtain qualitative and semi-quantitative compositional information. A summary of the main information
91 and references about this method is provided in Sect. 3.1. Instead, more details will be provided for the NRTI method, as this paper
92 aims to present recent advances in this technique at the ISIS facility, for its application in the field of Cultural Heritage. The qualitative
93 elemental composition obtained through both NRTI and NRCA has been compared with Particle-Induced X-ray Emission (PIXE)
94 analysis, which is a more established non-destructive method for quantifying the composition of archaeological objects made of a
95 wide range of matrixes [30, 31]. PIXE investigations have been conducted at the Grand Louvre Accelerator for Elemental Analysis
96 (NewAGLAE-ANR-10-EQPX-22)—Centre de recherche et de restauration des musées de France (C2RMF)—exploiting a 3-MeV
97 proton beam 50 μm wide and five SSD-EDX detectors for the PIXE mode. Details about the experimental conditions and the

Fig. 1 Pictures of the 8 crucible fragments analysed through neutron resonance absorption spectroscopy techniques. Metallic depositions are evident on the surface of some of these fragments, and the alloy colour suggests a composition related to brass



98 procedure followed for PIXE data analysis are described in [32]. The measurements of certified reference materials representing
 99 copper and copper alloys, such as BS938, NIST1107, CTIF-4, CTIF-5 and CTIF-6, were carried out for calibration purposes at the
 100 beginning and the end of each experimental session following the same protocol adopted for the archaeological samples. Errors can
 101 be estimated as in [33], with values ranging from 1 to 10%, depending on the concentrations.

102 3.1 Neutron resonance capture analysis

103 The NRCA technique relies on the Time-Of-Flight (TOF) measurement of the prompt γ -rays emitted after neutron captures reactions
 104 in the material under investigation [29, 34]. The arrival time of the γ cascade following the neutron capture reaction is recorded
 105 on the detector instead of performing full energy spectroscopy. Thus, the Time of Flight (and therefore the energy) of the neutron
 106 captured by the sample is determined. The resulting TOF spectrum is characterised by (n,γ) resonance absorption peaks, whose
 107 positions in time or energy are obtained for determining qualitative information about the sample elemental composition, as detailed
 108 in Sect. 3.2.

109 At the ISIS spallation source, NRCA experiments are routinely performed at the INES beamline with a detection set-up consisting
 110 of 3 yttrium aluminium perovskite (YAP) scintillator crystals coupled to silicon photomultipliers positioned above the sample stage
 111 at about 1 m distance from the sample position [21]. The resonant capture experimental set-up is optimised for providing a qualitative
 112 and semi-quantitative evaluation of the elemental composition of an object. NRCA is particularly useful for detecting impurities
 113 whose capture cross sections are very intense at low energies: even in the order of tens of parts per million (ppm) of elements with
 114 resonances between 1 and 10 eV can be detected [35] (for example, Au [21], AgSb and As which are of interest to Heritage Science). 4

115 3.2 Neutron resonance transmission imaging

116 The NRTI technique is an innovative extension of the Neutron Resonance Transmission Analysis (NRTA) [29, 34, 36] for conducting
 117 simultaneous spectroscopic and imaging analysis using a time- and space-resolved neutron detector. This method exploits the
 118 epithermal portion of a white neutron beam typically provided by a spallation source. For epithermal energies, resonance structures
 119 occur at distinct and at specific energies in the nuclide interaction cross sections with neutrons. Therefore, resonances can be used
 120 to identify and quantify the elemental, but also isotopic, composition of an object (Fig. 1). 5

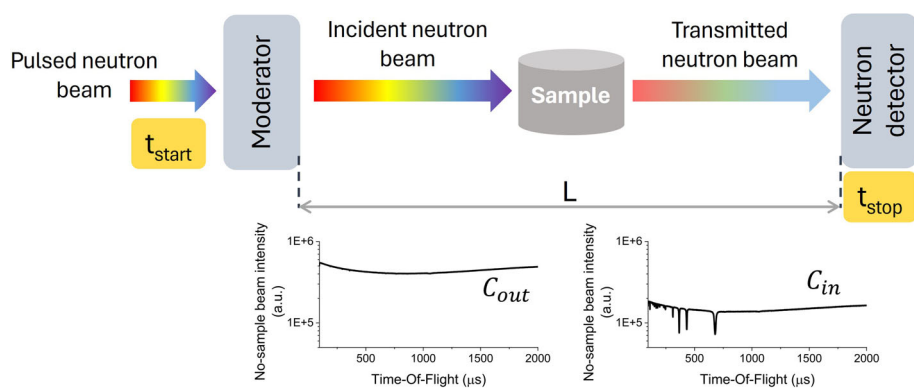
121 Spectroscopic information is collected through the TOF method, commonly used in a spallation source, and which relies on the
 122 measurements of the neutron arrival time on the detector relative to a trigger synchronised to the time of spallation (i.e. when the
 123 proton beam hits the target, the neutrons are produced by a spallation reaction). In this way, the neutron Time of Flights t can be
 124 converted into energies, in a non-relativistic regime:

$$E_n = \frac{mL^2}{2t^2}$$

127 where m is the neutron mass and L is the moderator to detector distance. L is calibrated using the main resonances of Gd and Ta
 128 foil samples, giving 23.44 m for this specific experimental campaign.

129 A schematic layout of the NRTI experimental set-up is represented in Fig. 2. In this case, the sample needs to be positioned as close
 130 as possible to the detector in order to reduce background noise due to scattering events and blurring due to the beam divergence.

Fig. 2 Schematic representation of the NRTI technique based on TOF measurements. Spectroscopy measurements are possible by tracing back the neutron velocity (and therefore energy) using the known neutron flight path L and its time of flight, calculated as the difference between the stop signal measured by the detector and the start signal synchronised with the proton pulse delivered by the source. An example of a neutron spectrum incident on the sample (C_{out}) and transmitted through (C_{in}) is reported in time coordinates. An example of negative peaks related to resonant neutron absorption can also be seen in the transmitted spectrum



131 Since NRCA and NRTI require different sample-to-detector positions, separate runs of measurements have been acquired. The
 132 typical structure of the transmitted neutron beam presents negative dips whose positions in time/energy correspond to the absorption
 133 resonances responsible for neutron removal from the incident beam. The position of these dips allows for elemental and isotopic
 134 identification through comparison with the total cross sections of elements available in a nuclear database. In this case, a web-based
 135 radionuclide database program named KAERI was used [37].

136 In each detector pixel, the transmitted neutron beam as a function of the neutron TOF is recorded, which is directly related
 137 to the theoretical transmission T representing the fraction of the neutron beam traversing the sample without any interaction.
 138 Experimentally, the transmission T can be derived by alternating measurements of the transmitted neutron beam with (C_{in}) and
 139 without the sample (C_{out}), with background correction for both detected spectra (B_{in} and B_{out}) and normalisation to the ratio M
 140 between the neutron irradiation currents on the sample and detector (in the absence of sample):

$$T = M \frac{C_{in} - B_{in}}{C_{out} - B_{out}}$$

143 NRTI measurements have been conducted at the INES beamline of the ISIS Neutron and Muon Source (UK), which is one of the
 144 beamlines providing a high epithermal component in the white neutron flux, placing a commercial neutron Gas Electron Multiplier
 145 (nGEM) [38, 39] in the beamline.

146 The active area of the detector is $10 \times 10 \text{ cm}^2$, and its pixel size is $0.8 \times 0.8 \text{ mm}^2$. However, the effective area of investigation is
 147 limited to the maximum opening size of the jaws (beam ‘delimiters’ made of neutron absorbing materials) present on INES, which
 148 is $4.0 \times 4.0 \text{ cm}^2$.

149 This detector is able to operate up to a total count rate of 10 MHz on the whole detector area. Moreover, each neutron is time
 150 stamped with a precision of 8 ns referred to the T_{zero} of the ISIS accelerator (i.e. the signal is synchronous to when the proton beam
 151 hits the target). Considering the time broadening of $\sim 400 \text{ ns}$ affecting the initial neutron pulse due to the neutrons slowing down in
 152 the small water moderator [40, 41], the time binning of the NRTI acquisition has been set at $1 \mu s$.

153 Considering the INES neutron flux reported in [42], the NRTI measurements of the crucible fragments lasted 2 days; each sample
 154 was irradiated for approximately 7 h, alternating acquisitions with and without the sample for normalisation purposes.

155 4 Results and discussion

156 At INES, NRCA is a routinely available technique, whereas NRTI is under development. Therefore, preliminary bulk elemental
 157 analysis was performed with NRCA to compare the NRTI results as both methods are based on TOF measurements of epithermal
 158 neutron absorption.

159 The NRCA spectra of the crucible fragments are shown in Fig. 3. The elements detected suggested the presence of bronze and
 160 brass alloys in the crucible fragments, with different amounts of secondary components like arsenic. The available TOF window
 161 of INES for useful NRCA signals is between 25 and $2000 \mu s$. Below $25 \mu s$, the background events (e.g. γ -flash coming from the
 162 source) are predominant over any useful signal peaks. Resonance capture peaks related to the presence of Cu and Zn are visible in
 163 the low TOF region ($25\text{--}180 \mu s$, see Table 1 for detailed positions and identification). Presence of Sn has been derived from the
 164 capture peaks at 38.8 and 109 eV and therefore occurring at 265 and $157 \mu s$, respectively (Fig. 3).

165 At higher TOF ($>200 \mu s$), the capture peaks of arsenic (46.9 eV/ $241 \mu s$) and silver (5.17 eV/ $725 \mu s$) have been identified as
 166 well as several peaks related to the presence of antimony in the $200\text{--}700\text{-}\mu s$ region ($660 \mu s/6.3 \text{ eV}$, $420 \mu s/15.4 \text{ eV}$, $356 \mu s/21.4 \text{ eV}$
 167 and $302 \mu s/29.8 \text{ eV}$). The qualitative composition derived through NRCA is averaged on the entire volume of the samples, except

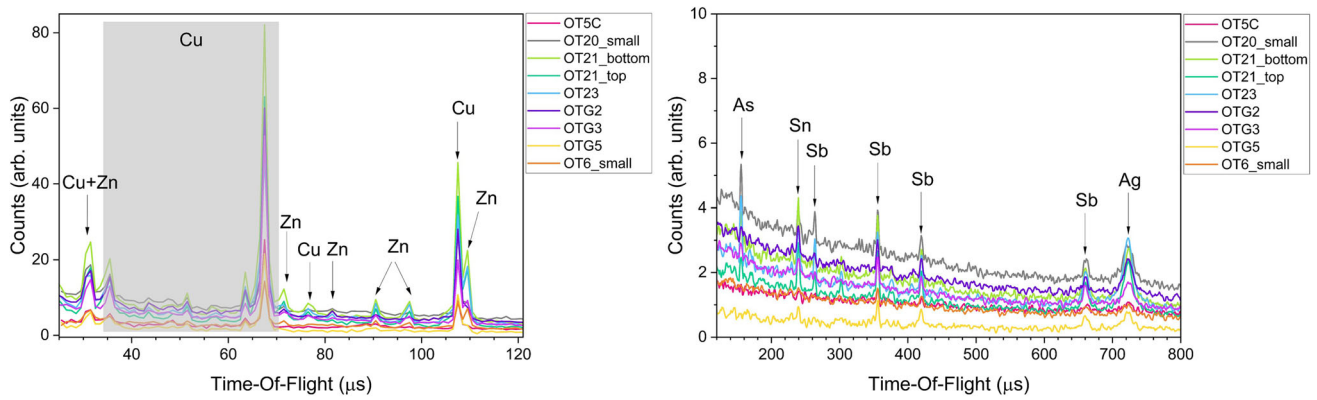


Fig. 3 NRCA spectra of the crucible fragments in the TOF region 25–120 μs and 120–1000 μs . The region between 1000 and 2000 μs has not been reported as it does not exhibit a significant signal for elemental composition determination. Main peaks related to copper, zinc, tin, arsenic, antimony, and silver are highlighted. Peaks within the grey box are related to copper. The qualitative composition of these fragments has been identified by comparing the resonance positions with capture (n, γ) cross-section libraries [37]

Table 1 Neutron resonance capture peaks of copper and zinc identified in the low TOF region (25–180 μs , visible in Fig. 3) with 1 μs of uncertainty and the relative positions converted in energy

Element	Resonant capture peak	
	TOF (μs)	Energy (eV)
Cu	32.3	2610
Zn	32.3	2610
Cu	34.6	2050
Cu	44.7	1360
Cu	52.3	994
Cu	58.1	806
Cu	64.6	651
Cu	68.6	578
Zn	78.0	447
Cu	82.2	402
Zn	91.7	323
Zn	98.0	280
Cu	108.7	230
Zn	110.4	223

168 for sample OT21, which is larger than the INES beam transverse size ($4.0 \times 4.0 \text{ cm}^2$). In this case, two separate measurements have
 169 been acquired (labelled as ‘top’ and ‘bottom’ in Fig. 3). Results are then averaged based on the effective irradiated volume, where
 170 both transverse sections measure $2.0 \times 2.0 \text{ cm}^2$.

171 The same elemental composition of the fragments has been disclosed by NRTI measurements, as shown in Fig. 4. Both techniques
 172 are transparent to the refractory material matrix, which ensures that the detection of metallic elements is not affected by any
 173 background signal that may be generated by the crucible matrix.

174 Moreover, in the case of NRTI, neutron Time of Flights lower than 20 μs are accessible without background interference.

175 The element distribution inside the volume of the crucible fragments can be mapped through NRTI by selecting the resonance of
 176 a specific nuclide in the transmitted spectrum. As an example, the distribution of Cu, Zn, Sn, Sb and Ag inside the bulk of sample
 177 ‘OT20_small’ is shown in this work. In particular, this crucible fragment does not have any extended metallic deposition visible on
 178 its surface (only a few microscopic droplets) and has a homogeneous thickness. Figure 5 shows the neutron radiography of fragment
 179 ‘OT20_small’ obtained through NRTI. Different levels of transmission can be seen due to a different composition inside the bulk.

180 By selecting the TOF/energy range of a specific resonance dip in the relative NRTI spectrum (Fig. 4), such as the Cu resonance
 181 around 2 keV, the contrast due to the absorption of neutrons by copper nuclei is enhanced in the 2D map, revealing the position of
 182 only copper inside the volume (Fig. 6). The same procedure can be made with resonances related to the other elements (Fig. 6), to
 183 facilitate the visualisation of the elemental distribution even for nuclide with similar neutron attenuation coefficient. Regarding the
 184 sample ‘OT20_small’, the following resonances have been selected, taking special account in selecting only those structures that do
 185 not overlap with other peaks of the other elements present in the bulk: 5.20 eV (Ag), 6.20 eV (Sb), 112 eV (Sn) and 515 eV (Zn).
 186 An example of the off-resonance selection is also provided to show that, with the selection of a region in the transmission spectrum

Fig. 4 NRTI spectra of the whole volume of the 8 crucible fragments shown in Fig. 1. Main peaks related to copper, zinc, tin, arsenic, antimony and silver are highlighted. Peaks within the grey box are related to a superposition of copper and zinc resonances. The qualitative composition of these fragments has been identified by indexing the resonance positions and comparing them with (n, tot) cross-section libraries [37]

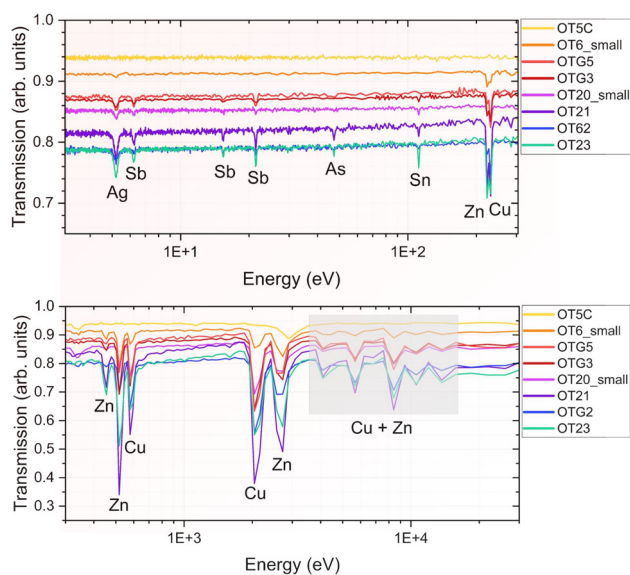
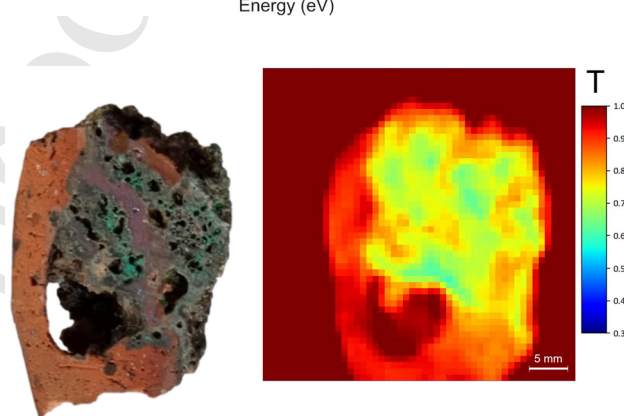


Fig. 5 Picture and transmission map of crucible fragment ‘OT20_small’. The size of the 2D map is $4.0 \times 4.0 \text{ cm}^2$



without resonant absorbing dips, it is no longer possible to distinguish the distribution of different elements, but only thickness and overall absorption effects are predominant.

A preliminary quantitative estimation of the Zn and Sn content in sample OT20_small can be made to assess the nature of the copper alloy present inside the fragment under consideration.

Considering the known relationship between the experimental transmission and the concentration of an element as reported in the literature [34], the concentration of detected elements in the whole volume has been estimated as follows: zinc 26%, tin 6%, antimony 1.6% and silver 0.3%; considering the presence of any other trace elements would not significantly alter the concentration of major elements such as zinc and tin. The uncertainties can be estimated at 15% since the integration routine is not fully optimised and the NRTI calibration is still in progress, with simulations to account for effects related to strong absorbing materials and thickness. A forthcoming publication detailing the calibration of the technique is currently underway.

The qualitative composition obtained through NRCA/NRTI and the quantification derived through NRTI have been compared with PIXE analysis, initially employed prior to neutron analysis to check the crucibles composition with a full optimised method for elemental composition analysis. PIXE is a non-destructive method more consolidated for the quantification of major, minor and trace elements in a wide range of sample matrixes. However, superficial metallic depositions that can be investigated with PIXE are present only on 4 crucible fragments (metallic layers on samples OTG5, OT23 and OT6_small and a few droplets on sample OT20_small). Table 2 contains the quantitative composition of several metallic spots, highlighting the complementarity between bulky neutron investigations and PIXE, which is limited to tens of micrometres in thickness [43]. In particular, in sample ‘OT20_small’, different droplets of metal can be traced back to copper and its contaminants, from which it is not possible to deduce brass or bronze production. NRCA and NRTI complete the picture of the composition: thanks to the fact that the entire fragments volume can be analysed and to the high interaction cross sections with certain elements, it was possible to recognise the presence of Zn and Sn even in small concentrations.

The quantification attempt using NRTI revealed a zinc and tin content that can be traced back to brass production. In addition, imaging performed through NRTI confirms the presence of brass in several areas, not visible by naked eye, more extensively than with small superficial analyses.

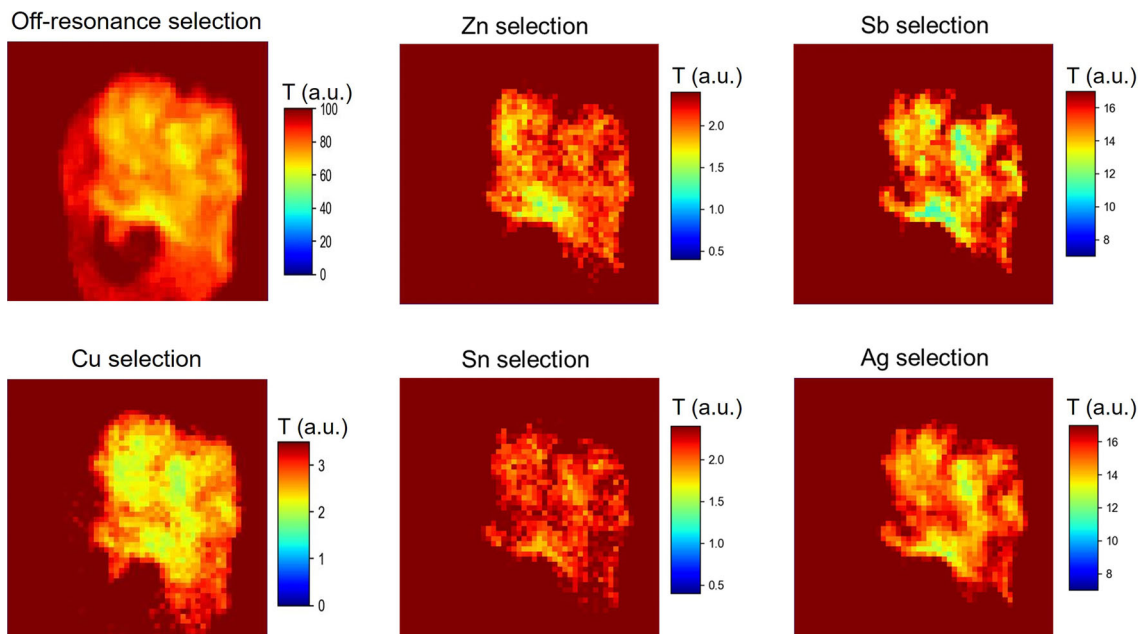


Fig. 6 NRTI maps after the selection of the main Zn, Sb, Sn, Cu and Ag resonances and of a TOF region without any absorption resonances. The size of all the 2D maps is $4.0 \times 4.0 \text{ cm}^2$

Table 2 PIXE composition (in ppm) of metallic depositions (droplets and more extended layers) of the crucible fragments ‘OT20_small’, ‘OTG5’, OT6_small’ and ‘OT23’

Sample	Description	Fe	Ni	Cu	Zn	Ga	As	Ag	Sn	Sb	Pb #L α
OT20_small	Metallic ‘drop’ #1	845	<i>u.d</i>	990,600	<i>u.d</i>	<i>u.d</i>	<i>u.d</i>	<i>u.d</i>	0	0	3300
OT20_small	Metallic ‘drop’ #2	846	586	990,200	0	0	<i>u.d</i>	<i>u.d</i>	<i>u.d</i>	<i>u.d</i>	3600
OT20_small	Metallic ‘drop’ #3	319	<i>u.d</i>	996,800	<i>u.d</i>	0	<i>u.d</i>	<i>u.d</i>	0	<i>u.d</i>	2430
OT20_small	Metallic ‘drop’ #4	332	<i>u.d</i>	994,200	<i>u.d</i>	<i>u.d</i>	<i>u.d</i>	<i>u.d</i>	0	<i>u.d</i>	2500
OTG5	Metallic ‘drop’ #1	1730	907	901,800	71,980	0	886	<i>u.d</i>	<i>u.d</i>	<i>u.d</i>	17,690
OTG5	Metallic ‘drop’ #2	1720	<i>u.d</i>	899,600	70,640	<i>u.d</i>	<i>u.d</i>	<i>u.d</i>	<i>u.d</i>	<i>u.d</i>	19,530
OTG5	Metallic layer	1610	609	902,700	69,640	0	894	532	2440	2760	17,700
OTG5	Metallic layer	1740	506	900,500	69,730	<i>u.d</i>	656	564	2200	2300	21,690
OTG5	Metallic layer	1690	491	886,000	67,370	0	1440	481	2170	2530	36,860
OT6_small	Metallic ‘drop’	2800	762	751,500	214,600	826	<i>u.d</i>	<i>u.d</i>	3440	0	22,130
OT6_small	Metallic layer	2890	834	750,100	214,200	0	<i>u.d</i>	<i>u.d</i>	3630	<i>u.d</i>	24,740
OT6_small	Metallic layer	2930	801	744,600	211,900	440	0	368	3980	1140	32,990
OT6_small	Metallic layer	2960	825	752,700	214,600	425	<i>u.d</i>	<i>u.d</i>	3840	1350	21,640
OT6_small	Metallic layer	1750	912	743,500	165,100	<i>u.d</i>	938	510	31,980	2300	56,870
OT23	Metallic layer	1800	844	734,400	162,500	0	1090	<i>u.d</i>	32,090	<i>u.d</i>	67,640
OT23	Metallic layer	1820	799	764,000	171,200	552	435	553	32,370	1640	30,400

Other elements not included in the table were not disclosed with PIXE (such as Mn, Co, In, Au, etc.). *u.d.* means below the detection limit. Errors can be estimated as in [33], with values ranging from 1 to 10%, depending on the concentrations

211 In this way, it is possible to confirm the presence of a workshop dedicated to the processing of brass in the ancient city of
 212 Mediolanum, since it is known from the literature that in Roman brass both tin and zinc are often present in the alloy [44].

213 Moreover, the detection through NRTI and NRCA of very small amounts of arsenic can be useful to characterise the alloy [45],
 214 as well as of Sb and Ag which may be present as contaminants of copper or other elements.

215 5 Conclusions

216 In the field of Heritage Science, neutron resonance absorption spectroscopy is a powerful method for determining non-destructively
217 the elemental composition of thick samples thanks to the high penetrating capability of neutrons and the presence of resonance
218 peaks in the neutron-induced absorption cross sections of nuclei. The application of these techniques can be now necessary for
219 non-destructive investigations of thick samples for which established probes such as X-rays cannot succeed. Neutron Resonance
220 Capture Analysis is a well-optimised elemental analysis and is routinely applied at the INES beamline of the ISIS Neutron and
221 Muon Source, but any capture peaks below 25 μ s are overshadowed by the background. On the other hand, Neutron Resonance
222 Transmission Imaging is an innovative and promising technique for determining both the elemental composition and the distribution
223 of the elements inside the bulk of archaeological objects, without the need for sampling, accessing in a complementary way the
224 region below 25 μ s (that is, the epithermal range between 4.6 keV and 30 keV approximately, where intense resonances occur for
225 several nuclides). The recent research conducted at the INES beamline of ISIS brought a dedicated measurement setup for NRTI
226 analysis using the nGEM detector, which enables measurements with better spatial resolution than previously performed.

227 The application of NRTI to crucible fragments related to brass production in the ancient Roman city of Mediolanum confirms
228 the presence of brass inclusions inside the volumes and succeeds in visualising their distribution even for those samples with no
229 superficial depositions that could be investigated by more conventional methods, such as PIXE. Furthermore, NRTI (and NRCA)
230 provided complementary results to the quantitative composition obtained through PIXE as arsenic, tin, antimony and silver can be
231 detected even in very small concentrations with neutron resonant absorption reactions. The detection of these elements can be useful
232 for characterising the alloy production process.

233 The NRCA investigation on the crucible fragments qualitatively confirms the overall elemental identification accomplished
234 through NRTI.

235 Moreover, this kind of samples presents an inhomogeneous distribution of Cu, Sn, Sb, Ag and As. Therefore, the feasibility
236 of the NRTI for localising the position of elements with enhanced contrast has been demonstrated through this case study. It was
237 also possible to provide a first attempt at quantifying the detected elements, as a result of the identification of a data normalisation
238 procedure adapted to the experimental set-up of INES and which is currently still being improved. More in-depth details on the
239 normalisation and quantification procedure will follow in a future publication.

240 To conclude, the achieved results demonstrate the usefulness of NRTI to perform non-destructive imaging combined with
241 elemental analyses for investigating the composition of inhomogeneous samples. Future steps will involve improving the NRTI
242 spatial resolution to be competitive with other neutron imaging techniques under this feature and the quantitative calibration. Making
243 NRTI a quantitative imaging technique can be a significant improvement in the field of neutron imaging methods. The access to
244 bulk elemental distribution with the potential to quantify the composition with a single technique can be a significant advantage for
245 non-destructive investigations of inhomogeneous objects that cannot be sampled (like those related to Cultural Heritage), providing
246 complementary details to more conventional (and superficial) analytical methods.

247 **Acknowledgements** This work was partially supported by the CNR-STFC Agreement (No. 2014–2020 and No. 2020–2027), concerning collaboration in
248 scientific research between the ISIS Neutron and Muon Source of STFC (UK) and CNR (Italy). Financial support by the Access to Research Infrastructures
249 activity in the Horizon 2020 Programme of the EU (IPERION HS H2020-INFRAIA-01-2018-19 G.A. n. 871034) is gratefully acknowledged (FIXLAB:
250 newAGLAE, France).

251 **Author contributions** G. M. and M.P. R. designed the research project to evaluate the feasibility of the NRTI technique for characterising the elemental
252 composition and distribution of the crucible samples. A. S. and G. M. performed neutron experiments and data analysis. Q. L. and G. M. carried out PIXE
253 measurements and data analysis. All authors gave contributions to the discussion of the result. G. M. wrote the manuscript in consultation with all authors.
254 All authors have read and approved the published version of the manuscript.

255 **Funding** H2020 Excellent Science, IPERION HS H2020-INFRAIA-01-2018-19 G.A. n. 871034, Giulia Marcucci.

256 **Data Availability Statement** This manuscript has associated data in a data repository.

257 **Declarations**

258 **Conflicts of interest** There are no conflicts to declare.

259 References

- 260 1. I.S. Anderson, R.L. McGreevy, H.Z. Bilheux, *Neutron Imaging and Applications A Reference for the Imaging Community* (Springer, New York, 2009).
261 (ISBN 978-0-387-78692-6)
- 262 2. M. Strobl et al., *J. Phys. D Appl. Phys.* (2009). <https://doi.org/10.1088/0022-3727/42/24/243001>
- 263 3. N. Kardjilov et al., *Mater. Today* **14**(6), 248–256 (2011). [https://doi.org/10.1016/S1369-7021\(11\)70139-0](https://doi.org/10.1016/S1369-7021(11)70139-0)
- 264 4. F. Salvemini et al., *Neutron News* **27**(2), 14–19 (2016). <https://doi.org/10.1080/10448632.2016.1163982>
- 265 5. N. Kardjilov et al., *Mater. Today* **21**(6), 652–672 (2018). <https://doi.org/10.1016/j.mattod.2018.03.001>
- 266 6. B. Schillinger et al., *J. Imaging* **4**(1), 22 (2018). <https://doi.org/10.3390/jimaging4010022>

- 267 7. D. Micieli et al., *Sci. Rep.* (2018). <https://doi.org/10.1038/s41598-018-30545-z>
- 268 8. N. Gelli et al., *Nucl. Inst. Methods Phys. Res. Sect. A Accel. Spectrom. Detect. Assoc. Equip.* **1051**, 168189 (2023). <https://doi.org/10.1016/j.nima.2023.168189>
- 269
- 270 9. A. Fedrigo et al., *J. Phys. Conf. Ser.* **2605**, 012019 (2023). <https://doi.org/10.1088/1742-6596/2605/1/012019>
- 271 10. S.W. Wilkins et al., *Nature* **384**(6607), 335–338 (1996). <https://doi.org/10.1038/384335a0>
- 272 11. M. Stapanoni et al., *Dev. X-Ray Tomogr.* **V 6318**, 63180F (2006). <https://doi.org/10.1117/12.679497>
- 273 12. M.P. Morigi et al., *Appl. Phys. A* **100**, 653–661 (2010). <https://doi.org/10.1007/s00339-010-5648-6>
- 274 13. M.P. Morigi et al., *J. Instrum.* **8**(08), C08010 (2013)
- 275 14. D. Mannes et al., *Phys. Procedia* **69**, 653–660 (2015). <https://doi.org/10.1016/j.phpro.2015.07.092>
- 276 15. F. Albertin et al., *Heritage* **2**(3), 2028–2038 (2019). <https://doi.org/10.3390/heritage2030122>
- 277 16. P.J. Withers et al., *Nat. Rev. Methods Primers* **1**, 18 (2021). <https://doi.org/10.1038/s43586-021-00015-4>
- 278 17. E. Perelli Cippo et al., *J. Anal. At. Spectrom.* **26**(5), 992 (2011). <https://doi.org/10.1039/c0ja00256a>
- 279 18. G. Festa et al., *J. Anal. At. Spectrom.* **30**(3), 745–750 (2015). <https://doi.org/10.1039/c4ja00384e>
- 280 19. A. Fedrigo et al., *J. Anal. At. Spectrom.* **34**(12), 2420–2427 (2019). <https://doi.org/10.1039/c9ja00300b>
- 281 20. L. Bartoli et al., *Metall. Italiana* **9**, 33–39 (2008)
- 282 21. A. Pietropaolo et al., *Appl. Spectrosc.* **64**(9), 1068–1071 (2010). <https://doi.org/10.1366/000370210792434440>
- 283 22. <https://www.isis.stfc.ac.uk>. Accessed 16th November 2023
- 284 23. A. Ceresa Mori, C. Cucini, in *Acta mineraria et Metallurgica. Studi in onore di Marco Tizzoni, Notizie Archeologiche Bergomensi*, 20, (Comune di Bergamo, 2012)
- 285
- 286 24. M. Tizzoni, *Notizie Archeologiche Bergomensi* **4**, 111–120 (1996)
- 287 25. J. Bayley, in *2000 Years of Zinc and Brass*, ed By P.T. Craddock (London: British Museum, 1998)
- 288 26. J. Bayley, al, in *Hidden Histories and Records of Antiquity. Essays on Saxon and Medieval London for John Clark, Curator Emeritus, Museum of London*, ed. By J. Cotton, J. Hall, J. Keily, R. Sherris, R. Stephenson (London: LAMAS , 2014) pp. 121–28
- 289
- 290 27. M. Martínón-Torres, T. Rehren, *Historical Metallurgy*, 36 (2002)
- 291 28. S. Merkel, *Metalla* **22**(1), 21–39 (2016)
- 292 29. P. Schillebeeckx et al., *J. Instrum.* **7**(03), 03009 (2012)
- 293 30. J. Salomon et al., *Nucl. Inst. Methods Phys. Res. Sect. B Beam Interact. Mater. Atoms* **266**(10), 2273–2278 (2008). <https://doi.org/10.1016/j.nimb.2008.03.076>
- 294
- 295 31. J. Salomon et al., *Appl. Phys. A* **92**, 43–50 (2008). <https://doi.org/10.1007/s00339-008-4512-4>
- 296 32. L. Pichon et al., *Nucl. Inst. Methods Phys. Res. Sect. B* **363**, 48–54 (2015). <https://doi.org/10.1016/j.nimb.2015.08.086>
- 297 33. M. Radepon et al., *Measurement* **114**, 501–507 (2018). <https://doi.org/10.1016/j.measurement.2016.07.005>
- 298 34. H. Postma, P. Schillebeeckx, *Neutron Resonance Capture and Transmission Analysis, Encyclopedia of Analytical Chemistry* (John Wiley & Sons Ltd, 2009) pp. 1–22
- 299
- 300 35. N. Kardjilov, G. Festa, *Neutron methods for archaeology and cultural heritage* (Springer Cham, 2017)
- 301 36. G. Noguere et al., *Nuclear Inst and Methods in Physics Research, A*, 575, 476–488 (2007)
- 302 37. <https://atom.kaeri.re.kr/>. Accessed 16th November 2023
- 303 38. F. Sauli, The gas electron multiplier (GEM): Operating principles and applications. *Nucl. Inst. And Meth. Phys Res A* **805**, 2–24 (2016)
- 304 39. <https://www.bbtech.co.jp/en/products/ngem/>
- 305 40. G. Škoro, S. Lilley, R. Bewley, *Phys B Phys Condens. Matter* **551**, 381–385 (2018). <https://doi.org/10.1016/j.physb.2017.12.060>
- 306 41. P. Schillebeeckx, H. Postma, Neutron resonance analysis methods for archaeological and cultural heritage applications. In: D’Amico, S., Venuti, V. (eds) *Handbook of Cultural Heritage Analysis* (Springer, Cham, 2022). <https://doi.org/10.1007/978-3-030-60016-7>
- 307
- 308 42. C. Cazzaniga et al., *AIP Adv.* **11**(7), 075005 (2021). <https://doi.org/10.1063/5.0043935>
- 309 43. A. Subercaze et al., *Nucl. Inst. Methods Phys. Res. Sect. B* **406**, 104–107 (2017). <https://doi.org/10.1016/j.nimb.2017.02.014>
- 310 44. P.T. Craddock, *J. Archaeol. Sci.* **5**(1), 1–16 (1978). [https://doi.org/10.1016/0305-4403\(78\)90015-8](https://doi.org/10.1016/0305-4403(78)90015-8)
- 311 45. A. Pollard et al., *Antiquity* **89**(345), 697–713 (2015). <https://doi.org/10.15184/aqy.2015.20>

Springer Nature or its licensor (e.g. a society or other partner) holds exclusive rights to this article under a publishing agreement with the author(s) or other rightsholder(s); author self-archiving of the accepted manuscript version of this article is solely governed by the terms of such publishing agreement and applicable law.

Author Query Form

**Please ensure you fill out your response to the queries raised below
and return this form along with your corrections**

Dear Author

During the process of typesetting your article, the following queries have arisen. Please check your typeset proof carefully against the queries listed below and mark the necessary changes either directly on the proof/online grid or in the 'Author's response' area provided below

Query	Details required	Author's response
1.	Please confirm if the author names are presented accurately and in the correct sequence (given name, middle name/initial, family name). Author 1 Given name: [Maria Pia] Last name [Riccardi]. Also, kindly confirm the details in the metadata are correct.	
2.	Kindly check and confirm whether the corresponding author is correctly identified.	
3.	Kindly check and confirm the country name is correctly identified for affiliation 4.	
4.	Please check the clarity of the sentence 'NRCA is particularly ... can be detected'.	
5.	Please check and confirm the inserted citation of Figure 1 is correct. If not, please suggest an alternative citation. Please note that figures should be cited in sequential order in the text.	